ORIGINAL PAPER

Multiple Scratching: An Atomistic Study

Iyad Alabd Alhafez[1,2] · Michael Kopnarski[1,3] · Herbert M. Urbassek[1]

Abstract

Using molecular dynamics simulation, we investigate multiple scratching processes in which a tip moves through a groove that has already been formed during a previous scratch. We use a conical indenter such that the friction coefficient is independent of the scratch depth. First, a single scratch to a depth of 4 nm is compared with a 2-cycle scratch in which a scratch at depth 2 nm is followed by a second scratch to the full depth of 4 nm. We observe that the second cycle shows a smaller friction coefficient as long as the tip moves through the pre-formed groove without touching the front end. In addition, we studied 5 cycles of scratching, in which the scratch depth was increased by 2 nm in each cycle. These results confirm and generalize the findings for the 2-cycle scratch. A constant-load 2-cycle scratch simulation emphasizes that the reduction in transverse load—and, consequently, in the friction coefficient—is caused by the fact that, despite a large normal area supporting the normal load, only a thin area is available to resist the transverse movement of the scratch tip. The work done during scratching is in good approximation proportional to the scratch volume showing that the transverse hardness is approximately constant in all scratch processes investigated here.

Keywords Nanoscratching · Friction · Molecular dynamics · Hardness

1 Introduction

Molecular dynamics simulations have been frequently used to study surface scratching on an atomistic basis. Such studies have been performed mostly for metallic samples, but also for ceramic materials and metallic glasses [1–13]. As a result, information on the mechanisms of plastic deformation in these samples was obtained [11, 14] that is useful for applications such as ultra-precision machining [15, 16].

As a rule, simulations study single scratches. In applications, however, often multiple scratches are used in which the scratch tip runs repeatedly over the same scratch groove, either on a closed circular path or repeatedly in a reciprocating motion from one end of the scratch groove to the other and back again. The processes occurring under such multiple scratches have up to now rarely—to our knowledge: not at all—been investigated using molecular dynamics simulation. This is in contrast to studies of multiple nanoindentation, which have been performed to investigate the changes in the mechanical response of the (multiply) indented sample [17, 18]. In other simulational studies, the plastic deformation beneath a scratch groove [19] or of a volume filled with a density of dislocations [20] have been explored by nanoindentation simulation.

In the present paper, we study such a multiple scratch scenario for an elemental metal, bcc Fe. We use displacement-controlled simulations [21], in which the path of the scratch tip is prescribed, and the resulting forces are determined from the simulation. We therefore increase the depth of scratch after each scratch cycle. A conical tip is used, whose self-similar form guarantees that the friction coefficient is independent of the scratch depth.

Three simulation scenarios are performed. In the first scenario, a single scratch to a depth of 4 nm (denoted as the *single scratch*) is compared to a twofold scratch, in which the scratch tip first scratches at 2 nm depth, then reverses its motion and scratches back at 4 nm depth. This latter scratch

✉ Herbert M. Urbassek
 urbassek@rhrk.uni-kl.de
 http://www.physik.uni-kl.de/urbassek/

[1] Physics Department and Research Center OPTIMAS, University Kaiserslautern, Erwin-Schrödinger-Straße, 67663 Kaiserslautern, Germany

[2] Institute of Applied Mechanics, Clausthal University of Technology, Adolph-Roemer Str. 2A, 38678 Clausthal-Zellerfeld, Germany

[3] Institut für Oberflächen- und Schichtanalytik IFOS GmbH, Trippstadter Straße 120, 67663 Kaiserslautern, Germany

is denoted as the *2-cycle scratch*. In a second scenario, a series of 5 scratch cycles is studied, in which the scratch depth is increased by 2 nm in each cycle. The comparison of the single and the 2-cycle scratch as well as the analysis of the change of the forces and the developing plasticity with cycle number allows us to draw conclusions on the differences between single and multiple scratches. Finally, we adapt the second cycle in the *2-cycle scratch* such that the normal load is approximately identical to that in the first cycle. This *constant-load* scratch allows us to extend our results to a scenario that is closer to the experimental situation.

2 Method

The sample is a bcc Fe crystal with a (100) surface; its sides are aligned with the [010] and [001] crystal axes. The crystal has lateral sizes of 74.8 nm × 85.0 nm and a depth of 41 nm, see Fig. 1a, and consists in total of 22,407,812 atoms. The conical tool is built of a rigid array of 727,524 carbon atoms; it has a semi-apex angle of $\theta = 60°$. It is hollow with a thickness of approximately 10 Å. As Fig. 1b shows, it has been cut out of a diamond carbon lattice and has an atomically sharp apex.

The Mendelev potential [22] describes the interaction between Fe atoms. By fixing two atomic layers at the lateral and bottom sides, translational motion of the substrate during indentation and scratching is prevented. A velocity-scaling thermostat [23] keeps the adjacent 4 layers at a prescribed low temperature, < 10 mK, in order to allow for easier identification of dislocations. The interaction between the C atoms of the tip and the Fe atoms of the sample is modeled by a Lennard-Jones potential [24] that has been cut off at its minimum at 4.2 Å [25] and is then shifted such as to have continuous energy and force at the cut-off radius.

The simulations are performed by indenting the tool to a depth d with constant velocity v. After a hold phase of 50 ps, the tool is then moved along the [010] crystal direction for a total scratch length of 15 nm. For single scratch, the simulation terminates here. Both for indentation and for scratching, the tool velocity amounts to $v = 20$ m/s. We use displacement-controlled simulations [21], in which the path of the scratch tip is prescribed, both during the nanoindentation and the scratch phase. We note that recently load-controlled simulations for nanoindentation have been performed [26, 27], but to our knowledge not yet for scratching.

For multiple scratching, after a hold phase of 50 ps the above routine is repeated; this means, the tool is again indented further into the material and the scratch process is repeated. Note that the direction of scratch is inverted ('reciprocating motion'). The 'scratching distance' used to quantify our results is, however, always measured from the indentation point, at which the scratch cycle starts. The indentation, scratching, and retraction stages of the tool motion are illustrated schematically in Fig. 1a.

Simulations are performed with LAMMPS [28] with a constant time step of 1 fs. The software tool OVITO [29] is employed to visualize the atomistic configurations. This tool allows, in particular, to identify dislocations, to determine their Burgers vectors $\boldsymbol{b}$, and to measure the total length of the dislocation lines, L_{disl}.

3 Results

3.1 Single Scratch to 4 nm

Let us first discuss the results for the single scratch to 4 nm. Fig. 2 shows the normal force, F_n, and the transverse force, F_t, as well as the friction coefficient,

$$\mu = F_t/F_n. \tag{1}$$

Immediately after indentation, the transverse force is close to zero. It rises to an approximately stable value of around 0.7 μN, which is reached after around 4 nm of scratching. This onset regime is typical of scratching simulations. The

Fig. 1 Schematics of the simulation setup. **a** A conical tip of semi-apex angle $\theta = 60°$ indents the surface to a depth d and scratches it to a length of $L = 15$ nm. At the end point, it reverses orientation and scratches backward. **b** Close-up view of the tip as seen from the scratching direction
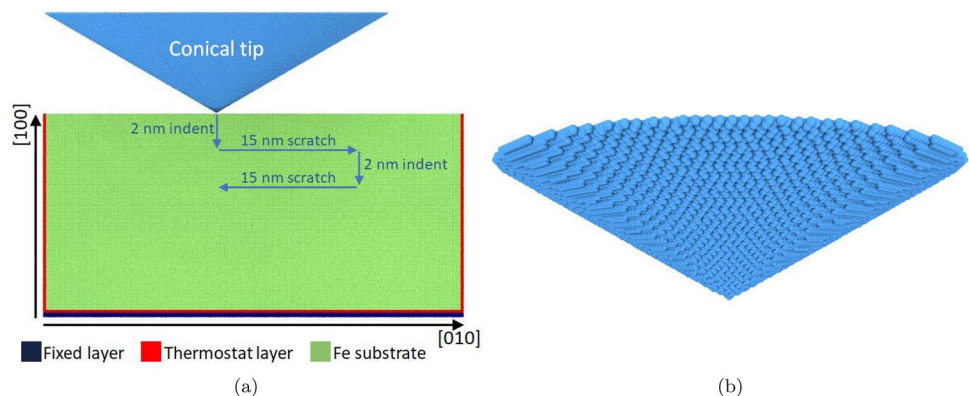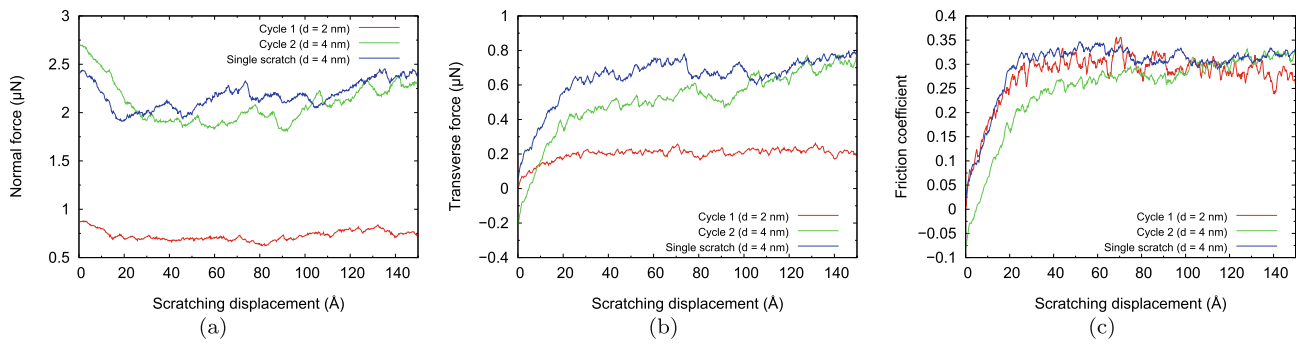
Fig. 2 Comparison of a single scratch at depth $d = 4$ nm with a scratch to $d = 2$ nm (cycle 1) and a second scratch (cycle 2). Normal (**a**) and transverse (**b**) forces as well as friction coefficient (**c**) as a function of scratching length

steady-state phase after 4 nm scratching shows strong fluctuations which are caused by bursts of dislocation nucleation and emission [14, 30]. The normal force, in contrast, is quite stable throughout the scratching, apart from the dislocation-induced fluctuations mentioned above.

The friction coefficient, in consequence, shows an approximately constant behavior after the onset phase; an average over scratching from 4 to 15 nm gives $\mu = 0.31$. Note that μ fluctuates considerably less than F_n and F_t; this is because dislocation nucleation and emission events affect both the normal and the transverse force similarly, such that these fluctuations largely cancel in μ.

The friction coefficient of a conical indenter can be assessed by the ratio of the (projected) normal and transverse contact areas A_n and A_t as $\mu = A_t/A_n$ [31]; this approximation is based on the assumption that the material hardness in transverse and normal direction are the same. For a conical tip, this gives

$$\mu = \frac{2}{\pi \tan \theta} = 0.37 \tag{2}$$

in reasonable agreement with our simulation result. Note that a systematic molecular dynamics study of scratching

with a conical tip showed similarly good agreement of the simulated friction coefficients with Eq. (2) for a wide range of semi-apex angles, from 30° to 70° [11].

3.2 2-Cycle Scratch to 4 nm

In the 2-cycle scratch, the tip first scratches at a depth of $d = 2$ nm (cycle 1), then indents to depth $d = 4$ nm and reverts its path to complete the scratch to $d = 4$ nm (cycle 2). We sketch schematically this process in Fig. 3a; the top view shows the grooves carved out during the first and the second cycles. Here also the onset and steady-state phases of the scratch are marked as well as an 'end phase' that will become important for cycles beyond the first cycle.

Figure 2 demonstrates that the normal force for cycle 2 is approximately identical (average over scratching from 9.5 to 15 nm: 2.18 μN) to that for the single 4-nm scratch (average of 2.27 μN). This is a factor of around 3 larger than the normal force in the first cycle (average of 0.76 μN). For a constant material hardness, one expects that the normal force rises proportional to the normal contact area

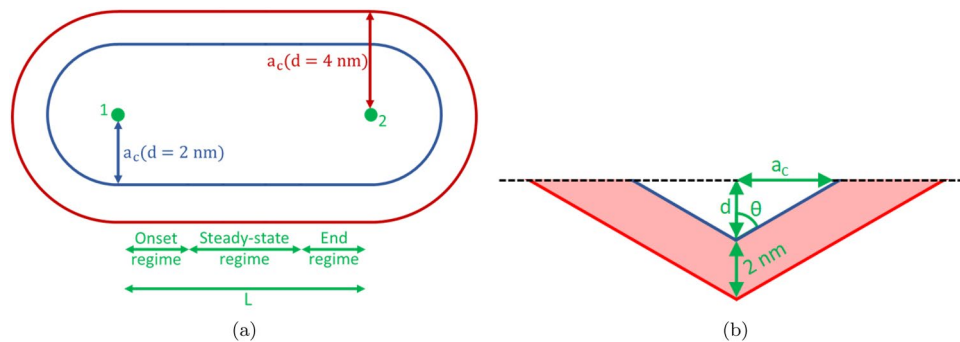**Fig. 3** Schematic **a** top view and **b** side view of 2-cycle scratching. In **a** the first indent to depth $d = 2$ nm is at position 1, during scratch the blue groove is carved out and the tip ends at position 2. There, the tip indents to 4 nm and scratches back from 2 to 1. The contact radii

a_c for the 2 scratches are indicated. For the first scratch the onset, steady-state and end regimes are marked; see text. In the side view, the transverse area ΔA, Eq. (10) of the second scratch is colored red

$$A_n = \pi a_c^2 = \pi (d \tan \theta)^2, \tag{3}$$

and hence $F_n \propto d^2$. Here, the radius of the contact area is given by

$$a_c = d \cdot \tan \theta. \tag{4}$$

The weaker increase observed in the simulation is caused by the high dislocation densities created for the shallowest scratch, cf. Sect. 3.3 below, which increase material hardness. This effect has been found already previously in scratch simulations with both spherical [9] and conical tips [11] and is related to the so-called indentation size effect [32–34].

The transverse force, F_t, shows a peculiar behavior.

1. The transverse force for cycle 2 shows *negative* values at the start of the simulation. This is caused by the asymmetric situation of the tip during and after indent: the material at the higher side extends up to the original surface and exerts an (elastic) lateral pressure on the tip toward the lower side of the material which is bounded by the groove bottom.
2. For cycle 2, F_t is systematically below that for a single scratch to 4 nm in the first 10 nm of scratch. This is caused by the fact that only the lowest 2 nm of the tip are loaded in frontal direction by the sample material; the upper part of the tip is free since it scratches in the groove already laid free in cycle 1. Only the lateral parts of the tip feel the full resistance of the material throughout the full immersed depth of 4 nm.
3. In the last 5 nm of scratch, the transverse force is identical to that in the single-cycle scratch. Along this path, the frontal part of the tip is fully immersed in the sample in front of the groove excavated during cycle 1. Using the cone's semi-apex angle of $\theta = 60°$, the cone touches the front part of the groove at a distance of $d \tan \theta = 7$ nm; since the 2-nm groove has tilted ends, the full material resistance builds up only at a smaller distance to the cycle end. We denote this stage as the 'end regime' of a cycle.

The friction coefficient follows the behavior of the transverse force, and exhibits too small values in the onset and steady-state regimes of the cycle compared with the single-cycle scratch and cycle 1. However, in the end regime—the final 5 nm of scratching – it assumes the same value as in the first cycle and in the single-cycle scratch.

One may inquire whether it costs less work to scratch to 4 nm depth with one or with two cycles. To answer this question, we calculate the scratch work as

$$W = \int F_t \, dx, \tag{5}$$

where the coordinate x points along the scratching path. We obtain $W = 9.66$ fJ for the single-cycle scratch and $W = 10.70$ fJ for the 2-cycle scratch, which splits up into 3.01 and 7.69 fJ for the first and second cycle, respectively.

We note that, from a macroscopic point of view, the scratch work and the scratch volume can be used to determine the scratch (or transverse) hardness. The argument runs as follows. The scratch volume is $V = A_t(d)L$ where the transverse contact area A_t is given by

$$A_t(d) = a_c d = d^2 \tan \theta. \tag{6}$$

Hence the transverse hardness, H_t, can be calculated from

$$H_t = \frac{W}{V}. \tag{7}$$

We note that V/W, the inverse of the transverse hardness, is often denoted as the wear coefficient in experimental scratch studies. Equation (7) yields $H_t = 28.9$ (23.2) GPa for the 2-nm (4-nm) scratch. The high value of the hardness for the 2-nm scratch is due to the high dislocation density for this scratch, discussed in Sect. 3.3.

These hardness values are quite large compared to the atomistically determined hardness, which is calculated by dividing the average transverse force, F_t, by the transverse contact area, A_t. The latter is determined directly from the simulation, by summing over the areas of the Fe atoms that are in contact (i.e., which feel the interaction force) with the scratch tip [10, 11, 35]. This atomistically calculated area is larger than the geometric area, Eq. (6), since (i) the repulsive interaction of the indenter extends farther out than the tip geometry, and (ii) also the pile-up contributes to the transverse area. An evaluation of the atomistic hardness, averaged over the last 8 nm of scratch, gives 17.9 GPa for the 2-nm scratch and 15.7 GPa for the 4-nm scratch. These values are in fair agreement with the previously determined value of 17.75 ± 1.15 for a 4-nm scratch [11].

We conclude that the shape of the first groove strongly influences the transverse force and the friction coefficient during the second scratch cycle. Toward the end of the cycle, the same values as in a single scratch are reached. However, in the steady-state regime of the second cycle, where the tip passes through the already excavated groove, the lateral force and the friction coefficient are systematically reduced.

3.3 Dislocation Network

Plasticity in our samples is dominated by dislocations; we found only negligible evidence for twinning. Fig. 4 displays the dislocation networks established at the end of scratching. The part of the network that is adherent to the scratch groove defines the plastic zone. Its shape can roughly be approximated as a semi-cylinder with its axis

aligned with the scratch direction [14]. The length Z of the semi-cylinder and its radius R_{pl} can be used to characterize the geometry of the plastic zone. The total length, L_{disl}, of dislocation lines within the semi-cylinder is used to determine the dislocation density within the plastic zone as

$$\rho = \frac{L_{disl}}{V_{cyl} - V_{groove}} \tag{8}$$

with the volume of the semicylinder $V_{cyl} = (\pi/2)R_{pl}^2 Z$ and the volume of the scratch groove V_{groove}. The simulation data are assembled in Table 1.

The plastic zone extends far beyond the scratch groove, both in axial and in radial direction. The cone has a contact radius a_c, Eq. (4), amounting to 3.5 (7) nm for $d = 2$ (4) nm; this gives the radial extension of the groove. Its length amounts to $15 + 2a_c = 21$ (29) nm for $d = 2$ (4) nm. Table 1 shows that Z surpasses the groove length by 50 %. The ratio of R_{pl} to a_c is denoted as the plastic-zone size factor,

$$f = R_{pl}/a_c, \tag{9}$$

and characterizes the plastic zone in radial direction. Its value is only 3.3 for the shallow scratch (cycle 1) but increases to around 5 for the deep scratch. Such values are common for both indentation and scratch into bcc materials [14, 21, 34]. The compact structure of the plastic zone for the 2-nm scratch (cycle 1) leads to a very high dislocation density. For the deeper scratches, the dislocation density is strongly reduced.

The differences in the plastic zone between the single-cycle and the 2-cycle 4-nm scratch are minor. The 2-cycle scratch leads to a (by 10 %) larger dislocation length contained in a (by 17 %) more compact plastic zone. This increase is caused by the interaction of the dislocations generated in cycle 2 with the dislocations left over from cycle 1. Such an increase has been observed previously when simulating indentation into a sample that contained pre-existing dislocations [20]. We conclude that the dislocation density for the 2-cycle scratch is somewhat increased compared to the single-cycle 4-nm scratch.

3.4 5 Cycles to 10 nm

In order to investigate whether the features found above for the 2-cycle scratch do also hold for further scratches, we extended the simulations to a total number of 5 cycles; in each cycle the scratch depth was increased by another 2 nm such that in the end, a total scratch depth of 10 nm was obtained. In these simulations, in order to save computation time, the hold phases after the indentation phase were ignored and only those after scratch were retained. We note that for the deeper scratches, the dislocation network approaches closer to the boundaries of the simulation volume. It is known that dislocations are not able to penetrate these rigid boundaries but are repelled from them; hence the complexity of the dislocation network generated in the simulation volume is increased [36]. We therefore do not evaluate the characteristics of the plasticity generated in the deeper scratches but focus on the discussion of the forces on the tip.
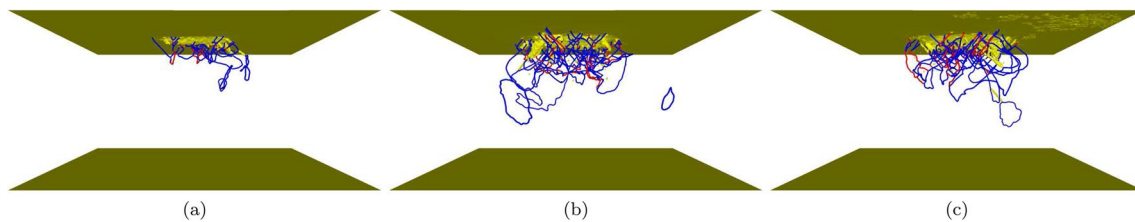

Fig. 4 Snapshots of the dislocation network formed at the end of the scratching process in the **a** single scratch to depth 2 nm (cycle 1) **b** double scratch, **c** single scratch to depth 4 nm. Yellow: deformed surface and bottom of the simulation volume. The transparent plane in **c** denotes the position of the original interface in the bilayer system. Dislocations are colored according to their Burgers vector $\boldsymbol{b}$: blue $\frac{1}{2}\langle 111 \rangle$, red $\langle 100 \rangle$

Table 1 Comparison of the characteristics of the plastic zone created in the single-cycle and the 2-cycle scratches. Z: length of the plastic zone

	Z (nm)	R_{pl} (nm)	f	L_{disl} (nm)	ρ (10^{16} m^{-2})
Cycle 1 ($d = 2$ nm)	31.6	11.5	3.3	305	4.81
Cycle 2 ($d = 4$ nm)	42.5	33.6	4.8	1191	1.61
Single cycle ($d = 4$ nm)	44.5	39.3	5.7	1076	1.01
Cycle 2 ($d = 2.3$ nm) constant load	29.1	10.7	2.7	381	7.31

R_{pl}: radius of plastic zone. f: plastic-zone size factor, Eq. (9). L_{disl}: total dislocation length within plastic zone. ρ: average dislocation density

Figure 5 shows the evolution of the normal and transverse force, as well as the friction coefficient over the 5 cycles. Averaged data are provided in Table 2. In detail we observe the following features.

1. In an initial onset stage—lasting around 4 nm—the normal force drops from its high value after indentation to a lower steady-state value while the tip scratches in the groove laid open in the previous scratches; simultaneously, the transverse force and the friction coefficient builds up from the initially negative values caused by the asymmetric initial situation.
2. A steady-state regime follows—from around 4 to 8 nm—in which the tip scratches in the groove laid open in the previous scratches. Here, the friction coefficient is smaller than the geometrical prediction, Eq. (2), since the tip only feels part of the transverse load.
3. Toward the end of the scratch—from 11 to 15 nm—the tip runs again into the virgin surface sample material. Here, the tip feels at all depths the geometrical friction coefficient, Eq. (2).
4. In an intermediate regime—from 8 to 11 nm— the scratch situation dynamically changes from the steady-state to the end regime. The lateral force increases more strongly than the normal force such that the friction coefficient increase toward its geometrical value.

In the steady-state regime from 4 to 8 nm, the friction coefficient assumes lower values for deeper scratches, because here the tip moves through the groove and the transverse resistance to scratching is raised only by a 2 nm thick region at the sides of the groove, while the normal load is also carried by the central area of the tip.

We conclude that qualitatively, the features observed and discussed after 2 cycles above, hold equally after multiple scratches, here for 5 cycles.

Table 2 Average normal (F_n) and transverse (F_t) forces as well as friction coefficient, μ, and work done W for scratching in the cycles 1–5

Averaged over 4–8 nm					
	Cycle 1	Cycle 2	Cycle 3	Cycle 4	Cycle 5
F_n (μN)	0.72	2.08	3.25	4.99	7.19
F_t (μN)	0.22	0.56	0.80	1.08	1.34
μ	0.30	0.27	0.25	0.22	0.19
W (fJ)	3.01	7.69	12.46	18.45	23.90

Data are averaged over the steady-state regime from 4 to 8 nm of the scratch

In order to discuss the dependence of the data, Table 2, with cycle number and hence with indentation depth more quantitatively, we plot them in Fig. 6 relative to their values in the first cycle. Figure 6a shows that the transverse force rises roughly linearly with cycle number and hence with indentation depth. This appears astonishing at first sight, since for a cone indented to depth d, the transverse area is proportional to d^2, Eq. (6). However, since in each cycle the indentation depth is only increased by 2 nm, the transverse area that can resist the scratching movement, is only

$$\Delta A = A_t(d) - A_t(d - 2\,\text{nm}) = 4\tan\theta(d - 1\,\text{nm}), \qquad (10)$$

and rises *linearly* with d, in agreement with our simulation data, Fig. 6a.

The normal force rises more strongly than the transverse force with cycle number, see Fig. 6b. This is due to the fact that the normal load is carried by both the groove and parts of the original surface; the area of the load carrying surface therefore scales with d^2 rather than d. As a consequence, the friction coefficient, $\mu = F_t/F_n$, decreases with cycle number, Fig. 6c.
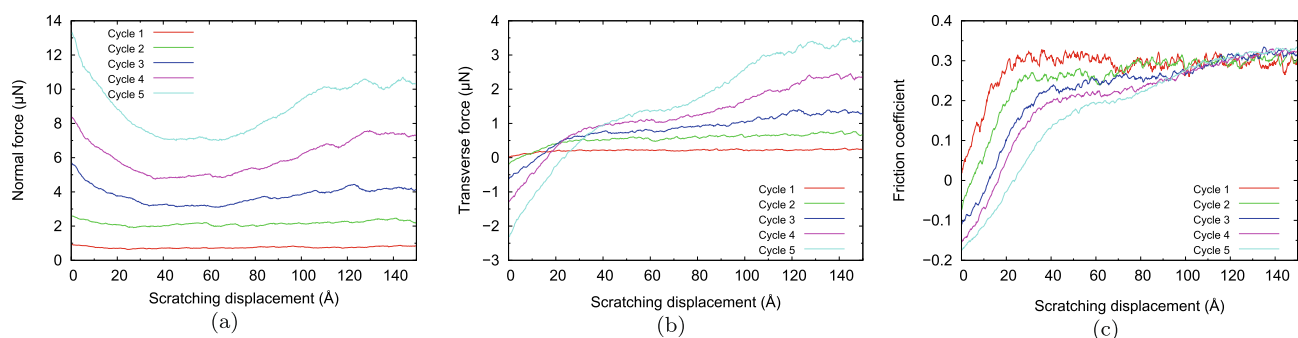

Fig. 5 Multiple scratch consisting of cycles 1–5 to a final depth of 10 nm. Normal **a** and transverse, **b** forces as well as friction coefficient, **c** as a function of scratching length
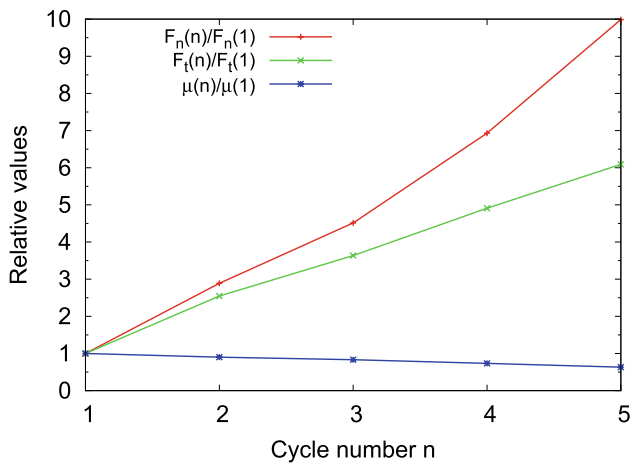
Fig. 6 Average normal (F_n) and transverse (F_t) forces as well as friction coefficient μ, vs cycle number n. Data are averaged over the steady-state regime from 4 to 8 nm of the scratch and plotted relative to their values in the first cycle

3.5 Second Cycle at Constant Load

In experiment, multiple-scratch studies are usually performed under constant load. We imitate such a constant-load scratch in the following way: At the end of cycle 1, we performed several test simulations for cycle 2 at different depths and measured the (average) normal load experienced during cycle 2. It turned out that if the simulation of cycle 2 is performed at a depth of 2.3 nm – i.e., increasing the indentation by only 0.3 nm—approximately the same normal load as in

cycle 1 is obtained. We therefore discuss here the results of a 'constant-load' 2-cycle simulation with indentation depths of 2 nm (cycle 1) and 2.3 nm (cycle 2). Figure 7a shows that the average load indeed reasonably coincides with that in cycle 1; the average—over the steady-state regime, 4–8 nm—amounts to 0.74 μN in cycle 2 compared to 0.72 μN in cycle 1.

The transverse force in this constant-load simulation is, however, strongly decreased compared to cycle 1, see Fig. 7b; its average is only 0.11 μN compared to 0.22 μN in cycle 1. This approximate halving of the transverse force is caused by the fact that the transverse force is carried by only a thin area, compare Fig. 3b and Eq. (10), while the normal force rests on the entire cross section of the cone. As a consequence, also the friction coefficient, Fig. 7c, is strongly reduced, from $\mu = 0.30$, Table 2, to only 0.15.

The work done in this constant-load simulation (cycle 2) amounts to 1.56 fJ. Using Eqs. (7) and (10), this corresponds to a transverse hardness of 23.2 GPa, in good agreement with the value obtained for the 4-nm scratch, Sect. 3.2.

The dislocation network after the constant-load scratch 2 is displayed in Fig. 7d. Due to the ejection of a dislocation loop, the second scratch homogenized the dislocation network. As shown in Table 1, the total length of the dislocation network only slightly increased, but it became more compact. Hence the dislocation density increased to above $7 \cdot 10^{16}$ m^{-2}, while the plastic-zone size factor decreased to only $f = 2.7$.

We conclude that constant-load multiple-scratch simulations lead to a large reduction of the transverse load—and,
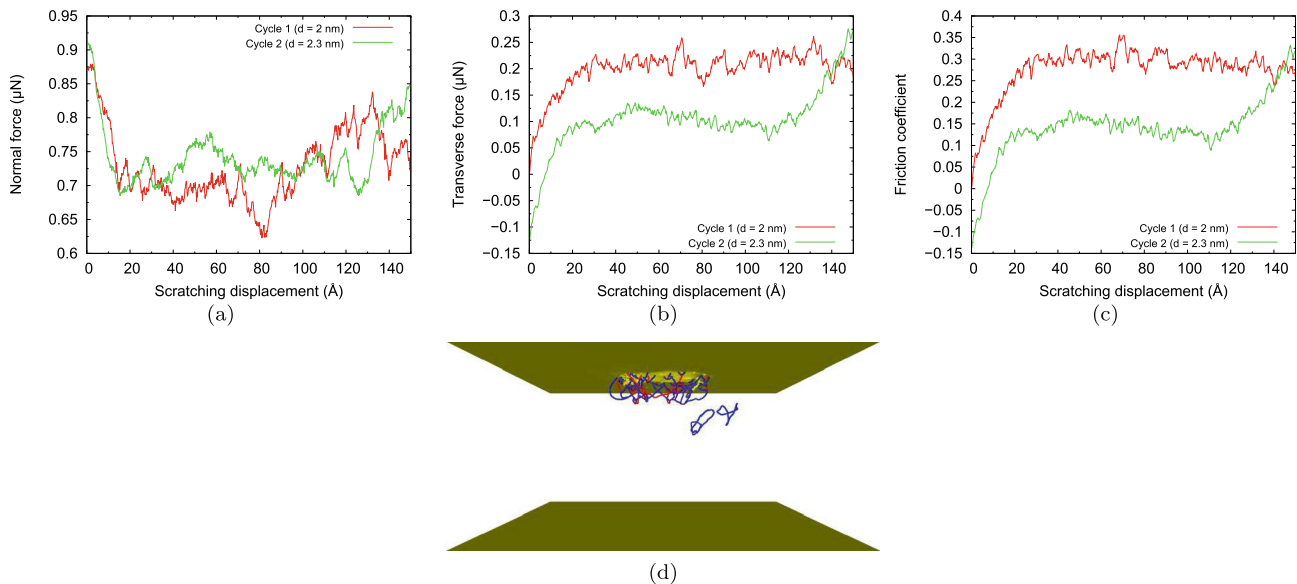

Fig. 7 2-cycle scratching at constant load: Data of the first cycle to depth $d = 2$ nm as in Fig. 2; the second scratch only scratches at $d = 2.3$ nm to keep F_n roughly constant. Normal (**a**) and transverse (**b**) forces as well as friction coefficient (**c**) as a function of scratching length. **d** shows a snapshot of the resulting dislocation network as in Fig. 4

consequently, of the friction coefficient—because despite a large normal area carrying the normal load, only a thin area is available to provide for resistance for the transverse movement of the scratch tip.

4 Summary

Multiple scratching requires that a tip moves through a groove that has already been formed during a previous scratch. By using a conical indenter, we made sure that the (geometrical) friction coefficient is independent of the scratch depth. We investigate the processes occurring during multiple scratching using several scenarios.

First, we compare a single scratch to a depth of 4 nm with 2-cycle scratch in which a scratch at depth 2 nm scratch is followed by a second scratch to the full depth of 4 nm. Here, we observed that the second cycle shows a reduced friction coefficient as long as the tip moves through the pre-formed groove without touching its front end. The plastic zone in the 2-cycle scratch is more compact but contains more dislocations since during the second cycle the tip interacts with the previously formed dislocations.

In addition, we studied 5 cycles of scratching, in which the scratch depth was increased by 2 nm in each cycle. This study confirmed the above features. In addition, it showed that in the steady-state regime, in which the tip scratches in the groove laid open in the previous scratches, the friction coefficient assumes ever lower values for deeper scratches due to the fact that while the central area of the tip carries the normal load, only the lateral 2 nm thick area of the tip offers resistance to transverse motion.

The work done during scratching is in good approximation proportional to the scratch volume; in other words, the transverse hardness is approximately constant in all scratch processes investigated here.

Finally, we performed a constant-load 2-cycle scratch simulation in order to emulate the conditions of common experimental scratch scenarios. Again, the systematics in the reduction of the transverse load—and, consequently, of the friction coefficient—were reproduced.

Author Contributions All authors contributed to the study conception and design. Simulations and data analysis were performed by IAA. The first draft of the manuscript was written by HMU. All authors commented on the manuscript and read and approved the final manuscript.

Declarations

Competing interest The authors have no competing financial or non-financial interests.

References

1. Komanduri, R., Chandrasekaran, N., Raff, L.M.: MD simulation of indentation and scratching of single crystal aluminum. Wear **240**, 113–143 (2000)
2. Mulliah, D., Christopher, D., Kenny, S.D., Smith, R.: Nanoscratching of silver (100) with a diamond tip. Nucl. Instrum. Meth. B **202**, 294–299 (2003)
3. Mulliah, D., Kenny, S.D., Smith, R., Sanz-Navarro, C.F.: Molecular dynamic simulations of nanoscratching of silver (100). Nanotechnology **15**, 243–249 (2004)
4. Jun, S., Lee, Y., Kim, S.Y., Im, S.: Large-scale molecular dynamics simulations of Al(111) nanoscratching. Nanotechnology **15**, 1169–1174 (2004)
5. Mulliah, D., Kenny, S.D., McGee, E., Smith, R., Richter, A., Wolf, B.: Atomistic modelling of ploughing friction in silver, iron and silicon. Nanotechnology **17**, 1807–1818 (2006)
6. Fang, T.-H., Liu, C.-H., Shen, S.-T., Prior, S.D., Ji, L.-W., Wu, J.-H.: Nanoscratch behavior of multi-layered films using molecular dynamics. Appl. Phys. A **90**, 753–758 (2008)
7. Lu, C., Gao, Y., Michal, G., Zhu, H., Huynh, N.N., Tieu, A.K.: Molecular dynamic simulation of effect of crystallographic orientation on nano-indentation/scratching behaviors of bcc iron. In: Luo, J., Meng, Y., Shao, T., Zhao, Q. (eds.) Advanced Tribology, pp. 562–563. Springer, Berlin (2010)
8. Mylvaganam, K., Zhang, L.C.: Nanotwinning in monocrystalline silicon upon nanoscratching. Scr. Mater. **65**, 214–216 (2011)
9. Gao, Y., Ruestes, C.J., Urbassek, H.M.: Nanoindentation and nanoscratching of iron: atomistic simulation of dislocation generation and reactions. Comput. Mater. Sci. **90**, 232–240 (2014)
10. Gao, Y., Brodyanski, A., Kopnarski, M., Urbassek, H.M.: Nanoscratching of iron: a molecular dynamics study of the influence of surface orientation and scratching direction. Comput. Mater. Sci. **103**, 77–89 (2015)
11. Alabd Alhafez, I., Brodyanski, A., Kopnarski, M., Urbassek, H.M.: Influence of tip geometry on nanoscratching. Tribol. Lett. **65**, 26 (2017)
12. Avila, K.E., Küchemann, S., Alabd Alhafez, I., Urbassek, H.M.: Nanoscratching of metallic glasses—an atomistic study. Tribol Int **139**, 1–11 (2019)
13. Lin, J., Jiang, F., Wen, Q., Yueqin, W., Jing, L., Tian, Z., Wang, N.: Deformation anisotropy of nano-scratching on c-plane of

sapphire: a molecular dynamics study and experiment. Appl. Surf. Sci. **546**, 149091 (2021)

14. Alabd Alhafez, I., Ruestes, C.J., Urbassek, H.M.: Size of the plastic zone produced by nanoscratching. Tribol. Lett. **66**, 20 (2018)

15. Hao, Z.P., Lou, Z.Z., Fan, Y.H.: Study on staged work hardening mechanism of nickel-based single crystal alloy during atomic and close-to-atomic scale cutting. Prec. Eng. **68**, 35–56 (2021)

16. Chen, X., Xiao, J., Zhu, Y., Tian, R., Shu, X., Jianfeng, X.: Micromachinability of bulk metallic glass in ultra-precision cutting. Mater. Des. **136**, 1–12 (2017)

17. Lodes, M.A., Hartmaier, A., Göken, M., Durst, K.: Influence of dislocation density on the pop-in behavior and indentation size effect in CaF_2 single crystals: Experiments and molecular dynamics simulations. Acta Mater. **59**, 4264 (2011)

18. Deldar, S., Alabd Alhafez, I., Smaga, M., Beck, T., Urbassek, H.M.: Cyclic indentation of iron: a comparison of experimental and atomistic simulations. Metals **9**, 541 (2019)

19. Zhang, J.J., Sun, T., Hartmaier, A., Yan, Y.D.: Atomistic simulation of the influence of nanomachining-induced deformation on subsequent nanoindentation. Comput. Mater. Sci. **59**, 14–21 (2012)

20. Alabd Alhafez, I., Ruestes, C.J., Bringa, E.M., Urbassek, H.M.: , Influence of pre-existing plasticity on nanoindentation: an atomistic analysis of the dislocation fields produced. J. Mech. Phys. Solids **132**, 103674 (2019)

21. Ruestes, C.J., Bringa, E.M., Gao, Y., Urbassek, H.M.: Molecular dynamics modeling of nanoindentation. In: Tiwari, A., Natarajan, S. (eds.) Applied Nanoindentation in Advanced Materials, pp. 313–345. Wiley, Chichester (2017)

22. Mendelev, M.I., Han, S., Srolovitz, D.J., Ackland, G.J., Sun, D.Y., Asta, M.: Development of new interatomic potentials appropriate for crystalline and liquid iron. Philos. Mag. **83**, 3977–3994 (2003)

23. Bussi, G., Donadio, D., Parrinello, M.: Canonical sampling through velocity rescaling. J. Chem. Phys. **126**, 014101 (2007)

24. Banerjee, S., Naha, S., Puri, I.K.: Molecular simulation of the carbon nanotube growth mode during catalytic synthesis. Appl. Phys. Lett. **92**, 233121 (2008)

25. Gao, Y., Urbassek, Herbert M.: Evolution of plasticity in nanometric cutting of Fe single crystals. Appl. Surf. Sci. **317**, 6–10 (2014)

26. Iteney, H., Cornelius, T.W., Thomas, O., Amodeo, J.: Load versus displacement-controlled nanocompression: insights from atomistic simulations. Scr. Mater. **226**, 115245 (2023)

27. Jaramillo, K.: Molecular dynamics simulation of force-controlled nanoindentation, University of Arkansas, Fayetteville Mechanical Engineering Undergraduate Honors Thesis (2015)

28. Plimpton, S.: Fast parallel algorithms for short-range molecular dynamics. J. Comput. Phys. **117**, 1–19 (1995)

29. Stukowski, A.: Visualization and analysis of atomistic simulation data with OVITO-the open visualization tool. Model. Simul. Mater. Sci. Eng. **18**, 015012 (2010)

30. Van Vliet, K.J., Li, J., Zhu, T., Yip, S., Suresh, S.: Quantifying the early stages of plasticity through nanoscale experiments and simulations. Phys. Rev. B **67**, 104105 (2003)

31. Bowden, F.P., Tabor, D.: Friction, lubrication and wear: a survey of work during the last decade. Br. J. Appl. Phys. **17**, 1521–1544 (1966)

32. Durst, K., Backes, B., Franke, O., Göken, M.: Indentation size effect in metallic materials: modeling strength from pop-in to macroscopic hardness using geometrically necessary dislocations. Acta Mater. **54**, 2547 (2006)

33. Pharr, G.M., Herbert, E.G., Gao, Y.: The indentation size effect: a critical examination of experimental observations and mechanistic interpretations. Annu. Rev. Mater. Res. **40**, 271 (2010)

34. Gao, Y., Ruestes, C.J., Tramontina, D.R., Urbassek, Herbert M.: Comparative simulation study of the structure of the plastic zone produced by nanoindentation. J. Mech. Phys. Sol. **75**, 58–75 (2015)

35. Ziegenhain, G., Urbassek, H.M., Hartmaier, A.: Influence of crystal anisotropy on elastic deformation and onset of plasticity in nanoindentation: a simulational study. J. Appl. Phys. **107**, 061807 (2010)

36. Alabd Alhafez, I., Ruestes, C.J., Gao, Y., Urbassek, H.M.: Nanoindentation of hcp metals: a comparative simulation study of the evolution of dislocation networks. Nanotechnology **27**, 045706 (2016)